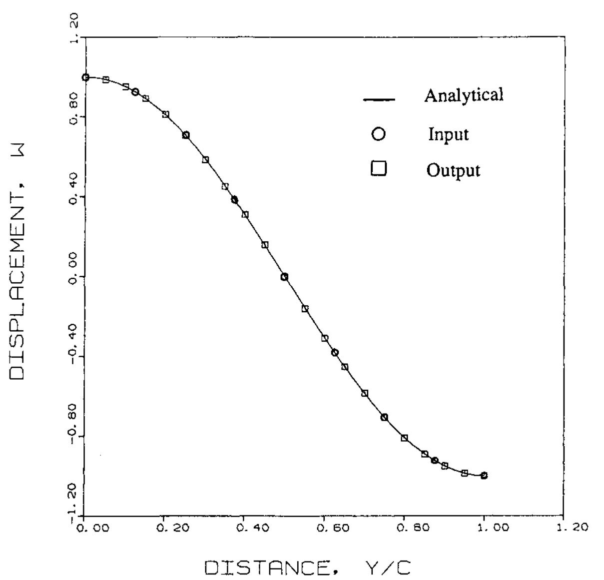

Fig. 4 Comparison of deformation along the aerodynamic grid line *CD*.

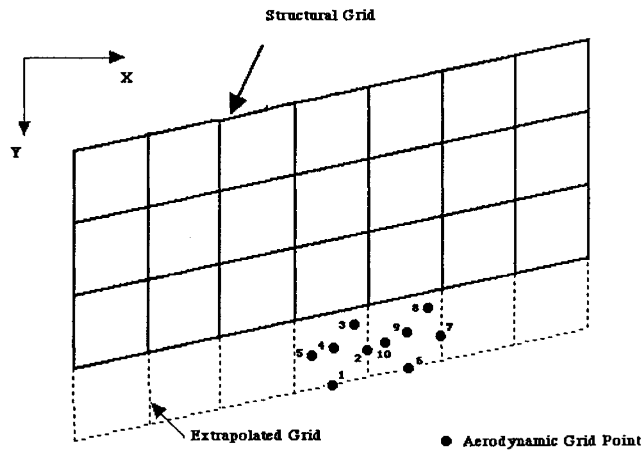

Fig. 5 Structural grid extrapolated to the control surfaces.

The displacements are calculated at the aerodynamic grid line AB by using three eight-node finite elements and the inverse mapping procedure. The displacements along the aerodynamic grid line AB are shown in Fig. 3 along with those calculated from Eq. (4). The solid line represents the displacements calculated using Eq. (4), and the circles represent the displacements used as inputs to the inverse mapping program. The square symbols denote the calculated displacement (output) from the inverse mapping procedure. It can be seen from Fig. 3 that the present results are in excellent agreement with the analytical solution. Similarly, the displacements calculated along the aerodynamic grid line CD using four eight-node finite elements for a constant value of x are shown in Fig. 4. Once again, a good agreement is found between the results obtained from the inverse mapping procedure and the analytical solution. Depending on the accuracy required, a larger number of elements are to be used for inverse mapping calculation along a particular aerodynamic grid point/line.

To show how the inverse mapping procedure can be used for obtaining the required data at the control surfaces/grid points, the problem shown in Fig. 5 was considered. The displacement for the problem shown in Fig. 5 is assumed as given by Eq. (4). The structural grid is extrapolated to the control surfaces using linear, quadratic, and cubic spline techniques. Using this extrapolated grid of two eight-node finite elements, the displacement is obtained at 10 different points over the control surface using the inverse mapping procedure. The percent error between the results from the inverse mapping and the analytical solution are summarized in Table 1 for different extrapolated schemes. It can be seen from Table 1 that the present approach gives the results with good accuracy.

Table 1 Percent error between the analytical solution and the inverse mapping procedure using different extrapolation schemes over the control surface grid points

Point Number	Linear	Quadratic	Cubic spline
1	1.53	0.00	0.00
2	1.07	0.16	0.00
3	0.81	0.15	0.07
4	0.97	0.13	0.01
5	0.92	0.08	0.06
6	1.53	0.30	0.00
7	1.08	0.16	0.00
8	1.09	0.43	0.35
9	0.97	0.13	0.01
10	0.76	0.08	0.22

Since isoparametric finite elements are used, any general wing configuration can be discretized. The inverse mapping procedure can be added to any of the existing finite element programs without any difficulty. The results presented indicate that the inverse mapping procedure is very accurate and efficient and, therefore, can be used for transforming any state variable (pressure, temperature, strain, etc.) between the aerodynamic and the structural grids.

References

[1]Schmitt, A. F., "A Least Squares Matrix Interpolation of Flexibility Influence Coefficients," *Journal of the Aeronautical Sciences*, Vol. 23, Oct. 1956, pp. 980.

[2]Rodden, W. P., "Further Remarks on Matrix Interpolation of Flexibility Influence Coefficients," *Journal of the Aerospace Sciences*, Vol. 26, Nov. 1959, pp. 760–761.

[3]Done, G. T. S., "Interpolation of Mode Shapes: A Matrix Scheme Using Two-Way Spline Curves," *Aeronautical Quarterly*, Vol XVI, Nov. 1965, pp. 333–349.

[4]Harder, R. L., and Desmarais, R. N., "Interpolation Using Surface Splines," *Journal of Aircraft*, Vol. 9, No. 2, 1972, pp. 189–191.

[5]Appa, K., Yankulich, M., and Cowan D. L., "The Determination of Load and Slope Transformation Matrices for Aeroelastic Analysis," *Journal of Aircraft*, Vol. 22, No. 8, 1985, pp. 734–736.

[6]Murti, V., and Vallippan, S., "Numerical Inverse Isoparametric Mapping in Remeshing and Nodal Quantity Contouring," *Computers and Structures*, Vol. 22, No. 6, 1986, pp. 1011–1021.

Effect of Thrust Vectoring on Level-Turn Performance

Pai-Hung Lee*
Aeronautical Research Laboratory,
Taichung, Taiwan 40722, Republic of China
and
C. Edward Lan†
University of Kansas, Lawrence, Kansas 66045

Introduction

In recent years, thrust vectoring has been actively considered as a means to improve a fighter's performance. Most

Received Nov. 8, 1990; revision received Jan. 4, 1991; accepted for publication March 8, 1991.

*Section Head.

†Professor, Aerospace Engineering. Associate Fellow AIAA.

frequently cited benefits include high angle-of-attack pitch and yaw controls,[1,2] and reduced takeoff and landing distances.[3] In Ref. 3, it was indicated that at a transonic Mach number of 0.9, thrust vectoring does not improve the sustained load factor in a level turn for the basic X-29 aircraft. However, the instantaneous turn performance can be improved.[3,4] In Ref. 4, an ideal aerodynamic model was used. In this Note, a more realistic aerodynamic model for an F-5E aircraft will be used to demonstrate the effect of thrust vectoring on all level-turn performance parameters (i.e., sustained load factor, rate of turn, and radius of turn) over a complete speed range. The objective is to show that the level of performance gain with thrust vectoring depends on the aerodynamics of the basic airframe and the thrust-weight ratio.

Method of Analysis

The load factor n is defined as the total lift (aerodynamic and vectored thrust) divided by weight

$$n = (L + L_T)/W \tag{1}$$

where L_T is the lift component from thrust vectoring and is given by

$$L_T = T\sin(\alpha + \delta_j) \tag{2}$$

In Eq. (2), the thrust deflection angle δ_j is measured relative to a body-fixed x-axis, and thrust T is assumed to be in the x-direction. From Eq. (1), the aerodynamic lift coefficient is found to be

$$C_L = (nW - L_T)/qS \tag{3}$$

Assuming a parabolic drag polar equation and equating the effective thrust to drag, it is obtained that

$$T_e = (C_{Do} + C_L^2/\pi Ae)qS \tag{4}$$

where

$$T_e = T\cos(\alpha + \delta_j) \tag{5}$$

Substituting C_L in Eq. (3) into Eq. (4) and solving for n, it is obtained that

$$n = \frac{q}{W/S}\sqrt{\frac{1}{k}\left(\frac{T_e}{qS} - C_{Do}\right)} + \frac{L_T}{W} \tag{6}$$

where $k = 1/\pi Ae$. Note that an optimal δ_j exists because the first term on the right side of Eq. (6) decreases and the second term increases as δ_j is increased. The rate of turn ψ and turn radius are still given by the conventional expressions[5]

$$\psi = g\sqrt{n^2 - 1/V} \tag{7}$$

$$R = V/\psi \tag{8}$$

Equation (6) is used when C_L is below the buffet onset. Above buffet onset, C_L is limited to the buffet lift coefficient C_{LB} so that Eq. (6) is replaced by

$$n_B = C_{LB}qS/W + L_T/W \tag{9}$$

On the other hand, at low speed C_L is typically limited by $C_{L\max}$. The limiting load factor is then given by

$$n_s = C_{L\max}\,qS/W + L_T/W \tag{10}$$

The lift coefficient is further limited by the structural load limit. In calculations, C_L is first evaluated from Eq. (4) at a given M. This C_L is then checked against aforementioned various limits before a final maximum n is calculated.

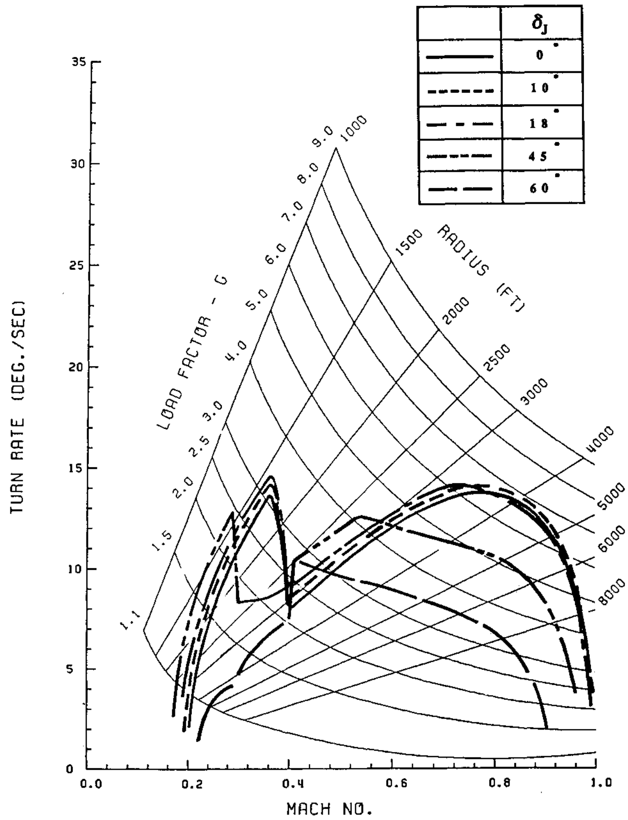

Fig. 1 Effect of thrust vectoring on sustained level-turn performance for a fighter aircraft (Altitude = 5000 ft, W = 13,000 lb, and sea-level thrust = 2 × 5000 lb).

It is observed that in Eq. (6) at given altitude, weight, and speed, the maximum load factor depends on the available thrust, Mach number M, and δ_j.

Numerical Results and Discussion

The method of analysis is applied to an F-5E at 5000-ft altitude. The maximum total thrust is 10,000 lb at sea level. Two weights, 13,000 lb and 10,000 lb having thrust-weight ratios of 0.77 and 1.0, respectively, will be considered. It is assumed that the induced aerodynamics from thrust vectoring for a fighter configuration can be ignored.[6] In addition, pitch trim can be maintained by some means.[6] Therefore, a point-mass model will be used in the following. This point-mass assumption is consistent with other existing analyses.The following results are based on existing aerodynamic data for an F-5E carrying two missiles without applying the maneuver flap. It is further assumed that for $M \le 0.35$, the aerodynamics are limited by $C_{L\max}$, while for $M \ge 0.4$, C_{LB} will be the limiting factor. For M between 0.35 and 0.4, the limiting C_L is interpolated between $C_{L\max}$ and C_{LB}. The values of k and C_{Do} are obtained by interpolating the experimental aerodynamic data with M. The available thrust is also interpolated with M and altitude. The structural load factor limit is assumed to be 7.33.

$T/W = 0.77$

The results of analysis are presented in Fig. 1. It is seen that there are two peak values for the turn rate. The low-speed values are produced by allowing C_L to reach $C_{L\max}$, not limited by C_{LB}. In the following, only the high-speed turn rate will be analyzed.

It is seen from Fig. 1 that $n_{\max} = 6.71$ at $M = 0.85$ without thrust vectoring ($\delta_j = 0$). On the other hand, $n_{\max} = 6.85$ at $M = 0.84$ with an optimal $\delta_j = 10$ deg. This represents a gain of 2%.

The maximum turn rate for $\delta_j = 0$ occurs at $M = 0.77$ with $\psi_{\max} = 13.7$ deg/s. However, at an optimal $\delta_j = 18$ deg, $\psi_{\max} = 14.1$ deg/s at $M = 0.73$ with a gain of 3%. Finally, the

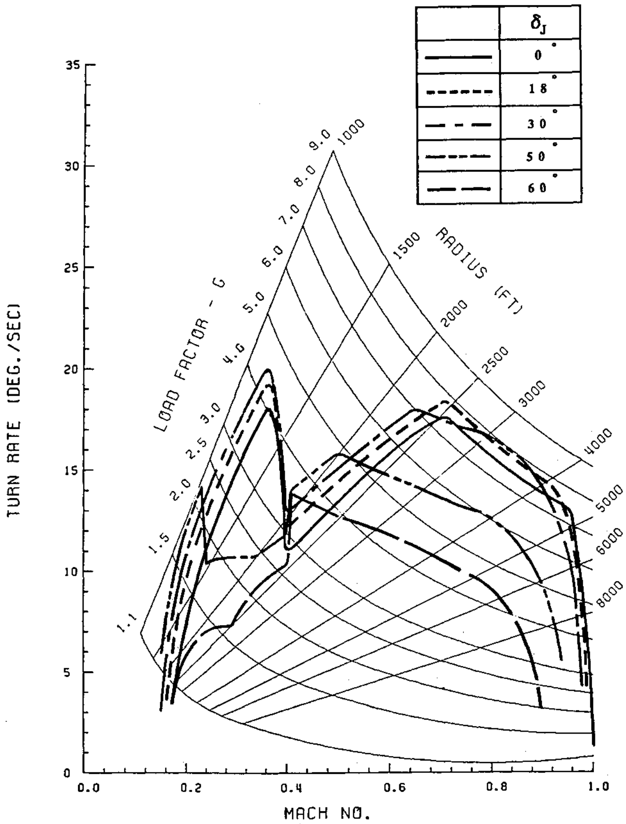

Fig. 2 Effect of thrust vectoring on sustained level-turn performance for a fighter aircraft (Altitude = 5000 ft, W = 10,000 lb, and sea-level thrust = 2 × 5000 lb).

minimum radius of turn is equal to 1670 ft with $\delta_j = 0$ at low speeds and is 1420 ft at an optimal $\delta_j = 45$ deg. It should be noted the $n_{\max}$ and $\psi_{\max}$ with thrust vectoring tend to occur at a lower Mach number than that without thrust vectoring.

***T/W* = 1.0**

The results are presented in Fig. 2. It is seen that without thrust vectoring, $n_{\max} = 7.47$ at $M = 0.82$, $\psi_{\max} = 17.5$ deg/s at $M = 0.71$ and $R_{\min} = 1250$ ft at low speeds. With thrust vectoring, $n_{\max} = 7.95$ at $M = 0.82$ and an optimal $\delta_j = 30$ deg; $\psi_{\max} = 18.4$ deg/s at $M = 0.71$ and an optimal $\delta_j = 18$ deg; and finally, $R_{\min} = 1020$ ft with an optimal $\delta_j = 50$ deg. These results represent a gain of 6% for $n_{\max}$ and 5% for $\psi_{\max}$.

As shown in the above results, the performance gain in level turn due to thrust vectoring depends not only on the basic airplane aerodynamics (e.g., C_{Do}, k, C_{LB}, $C_{L\max}$), but also on the available thrust-weight ratio as well as the structural limit load factor. However, the calculated performance gain is much less than that indicated in Ref. 4. In the latter, it was shown in descending turns that thrust vectoring provided about 20% improvement in turning time at high initial speeds. At low initial speeds, the improvement was small. This significant improvement in performance due to thrust vectoring is most likely the result of assuming a constant maximum aerodynamic load factor and ignoring compressibility effect on drag at high speeds. Therefore, more thrust can be utilized to augment the aircraft lift so that the turn rate is increased. In the present analysis, the maximum aerodynamic load factor is mostly limited by the buffet lift coefficients that decrease with Mach number. The effect of compressibility on C_{Do} and k has also been included by using the experimental data. Another difference is sustained performance being considered in the present analysis and instantaneous performance in Ref. 4.

Conclusions

A method of analysis was presented to determine the effect of thrust vectoring on level-turn performance. Calculated results based on the basic F-5E aerodynamics were presented. It was shown that different optimal thrust deflection angles existed for the sustained maximum load factor, turn rate, and minimum turn radius. Gains in maximum load factor and turn rate due to thrust vectoring were 2% and 3%, respectively, at a thrust-weight ratio of 0.77 at 5000-ft altitude. However, the corresponding gains were increased to 6% and 5% at a thrust-weight ratio of 1.0.

References

[1]Mason, M. L., and Burley, J. R., III, "Static Investigation of Two STOL Nozzle Concepts with Pitch Thrust-Vectoring Capability," NASA TP-2559, April 1986.

[2]Berrier, B. L., and Mason, M. L., "A Static Investigation of Yaw Vectoring Concepts on Two-Dimensional Convergent-Divergent Nozzles," AIAA Paper 83-1288, Seattle, WA, June 1983.

[3]Miller, E. H., "Performance of a Forward Swept Wing Fighter Utilizing Thrust Vectoring and Reversing," *Journal of Aircraft*, Vol. 23, No. 1, 1986, pp. 68–75.

[4]Schneider, G. L., and Watt, G. W., "Minimum-Time Turns Using Vectored Thrust," *Journal of Guidance, Control, and Dynamics*, Vol. 12, No. 12, 1989, pp. 777–782.

[5]Lan, C. E., and Roskam, J., *Airplane Aerodynamics and Performance*, Roskam Aviation and Engineering Corp., Ottawa, KS, 1988, p. 493.

[6]Paulson, J. W., Jr., et al., "A Review of Technologies Applicable to Low-Speed Flight of High-Performance Aircraft Investigated in the Langley 14×22-ft Subsonic Tunnel," NASA TP-2796, May 1988.

Transition of the Flutter Mode of a Two-Dimensional Section with an External Store

Zhi-chun Yang* and Ling-cheng Zhao†
Northwestern Polytechnical University, Xi'an, People's Republic of China

RECENTLY, Niblett[1] made a comprehensive study of the classical bending-torsion flutter, in which the flutter condition was related directly to the normal modes involved in flutter.

By using normalized eigenmodes and steady aerodynamics, the equation of motion of a wing is

$$\begin{bmatrix} 1 & \\ & 1 \end{bmatrix} \begin{bmatrix} \ddot{\xi}_i \\ \ddot{\xi}_j \end{bmatrix} + \begin{bmatrix} \omega_i^2 & \\ & \omega_j^2 \end{bmatrix} \begin{bmatrix} \xi_i \\ \xi_j \end{bmatrix} = \begin{bmatrix} c_{ii}q & c_{ij}q \\ c_{ji}q & c_{jj}q \end{bmatrix} \begin{bmatrix} \xi_i \\ \xi_j \end{bmatrix} \tag{1}$$

where ξ_i and ξ_j are the normal coordinates; ω_i and ω_j are the ith and jth eigenfrequencies, $\omega_i < \omega_j$, q is the dynamic pressure, and c_{ij} is the generalized aerodynamic coefficient obtained from the virtual work principle as

$$qc_{ij} = z_i L_j \tag{2}$$

with

L_j = the lift force associated with the jth mode
z_i = vertical displacement of the aerodyamic center associated with the ith mode

An explicit formula for the lower flutter critical dynamic

Received Nov. 15, 1989; revision received Oct. 15, 1990; accepted for publication March 27, 1991.

*Research Associate, Aircraft Engineering Department.

†Professor, Aircraft Engineering Department.